

# RECTIFICATION ALGORITHM OF CURVILINEAR EPIPOLAR GEOMETRY FOR SCENE DEPTH RETRIEVAL IN PLENOPTIC IMAGING SYSTEMS

M. Ardebili, A. Erdmann

CAU Kiel, Germany

## ABSTRACT

Here we present a novel algorithm for the rectification of sheared curvilinear epipolar lines in plenoptic cameras. The algorithm requires no advanced calibration procedure from state of the art approaches, but only knowledge that the distortions are uniquely radial in form. By considering Fresnel diffraction theory while exploiting wavefront symmetries, we've determined a generic set of conditions for the occurrence of radially distorted microimages. The microimage centres and radial distortion centres are further proven to be equivalent.

**Index Terms** — plenoptic, lightfield, imaging, microlens, microimage, radial, distortion, wavefront, aberrations, fresnel, diffraction

## 1. INTRODUCTION

The effect of main lens radial and depth distortions in a plenoptic camera with solutions to correcting for them through a metric calibration process are already proposed in literature with applications in both research and commercial uses [1], [2], [3]. An analytical expression for the depth accuracy was formulated [4]. A semi-analytical diffraction model is formulated for the aberration-free plenoptic camera, accounting for main lens vignetting [5]. With the use of ray-tracing for the plenoptic camera, rays are digitally reallocated to where they should ideally converge in the sensor plane to correct for lens aberrations [6]. This method utilises the concept of ray-space diagrams. The effect of aberrations however on image quality, has only been more recently investigated. Decentred microlenses have nodes in the field dependent Zernike coefficients that approximate the wavefront aberration function [7]. The problem of microimage distortions along with solutions to compensate for them is also a relatively new study. Distortions due to surface defects in the microlenses has been investigated [8]. We claim one particular source of microimage radial distortion is vignetting. A certain fractional occurrence of main lens vignetting inherently occurs and in combination with defocusing, introduces distortions that shear the epipolar lines on the local scale of the microimages. This may be especially pronounced for lower image redundancy. It is also important to appreciate the inevitable degradation on image quality that would occur as a result of aberrations. As shown in [9], using Schwartz's inequality, image contrast can never increase as a result of aberrations and will in general decrease contrast. Furthermore severe aberrations can limit the effective cut-off frequency.

Moreover, over certain frequency bands, aberrations can cause the optical transfer function (OTF) to become negative or complex valued, which gives rise to contrast reversal where intensity maxima vanish and vice versa [9].

Specifically, when aberrations translate into a merely radially symmetric deformation of the main lens caustic, consequent mirror

symmetries in the deformed wavefront aberration function of the microlenses emerge, independently of the arbitrary complexity of these final aberrations. These then cascade into radial distortions along the mirror axes of diffractive symmetry.

Assuming the conditions above hold, we mathematically prove from first principles the above claims in the *Lightfield Centroid Theorem (LFC)*. The proof utilises Fresnel diffraction theory [10] while exploiting wavefront symmetries as previously described. As the result holds true from the more accurate perspective of diffraction, it also holds true for classical geometrical optics.

A generic set of properties is thus established, under which microimage distortions are uniquely radial. The set constitutes the axioms for the algorithm. From the lightfield geometry, the coordinates of the radial distortion centre and microimage centre are derived and are shown to be equivalent. State of the art approaches require distortion rectification in the image formation process, through the use of polynomials, a lens surface error model or calibration targets [1], [6], [8], [3]. In contrast, our proposed depth retrieval algorithm merely requires distortions to be uniquely radial. To improve upon our algorithm's performance of depth estimation, through a geometrical construction, we introduce a suitable characteristic weighting function to evaluate a weighted arithmetic mean of baselines for an improved handling of outliers.

## 2. THE LIGHTFIELD CENTROID THEOREM (LFC)

[*Note:* In the following sections, all bold quantities refer to 2D position vectors measured from the optical axis (except  $\mathbf{u}$ ) and lie in planes perpendicular to the optical axis. Also for simplicity of notation, whenever we refer to a function  $f(x, y)$  of variables  $x, y$ , in a distinct coordinate frame,  $f(u, v)$  represents the re-expression of  $f(x, y)$  in terms of the variables  $u, v$ , while in general,  $f(x, y) \neq f(u, v)$ ].

### 2.1. Lemma

Let  $a$  be the main lens exit pupil to microlens entrance pupil distance along the main lens optical axis and let  $\mathbf{c}_e$  be the transversal centre coordinates of the main lens exit pupil, while  $\mathbf{x}'_o$  is the main lens real (or virtual) image. Then if  $\tilde{\mathbf{c}}_o$  is the chief ray intersection coordinates with the microlens entrance pupil plane  $\tilde{\Pi}$ , the distribution incident on this plane at polar coordinates  $(\rho, \phi)$  with respect to  $\tilde{\mathbf{c}}_o$  is given by  $U(\rho, \phi) = e^{-ik \tan(\alpha'_o) \rho \cos(\phi - \theta_o)} U_o(\rho)$  where  $U_o$  is the main lens axial APSF,  $k$  is the wavenumber of light and  $\alpha'_o$  is the zenith polar angle of the chief ray in image space.

**Proof:** The amplitude point spread function (APSF) incident on  $\tilde{\Pi}$  forms centred on  $\tilde{\mathbf{c}}_o$ . Thus the entrance pupil distribution at  $\mathbf{x}$  (with respect to the optical axis) where  $U_o$  is the main lens axial APSF, takes the form  $U(\mathbf{x}) = e^{i\frac{k}{a}(\tilde{\mathbf{c}}_o - \mathbf{c}_e) \cdot \mathbf{x}} U_o(\mathbf{x} - \tilde{\mathbf{c}}_o)$ .

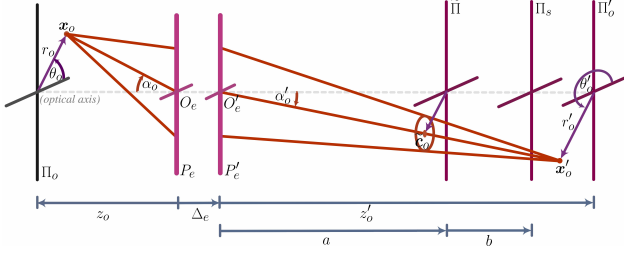


**Figure 1:** Depiction of the imaging model for the main lens with general distortion. For simplicity of illustration, entrance and exit pupil centres coincides with the optical axis. The entrance and exit pupil planes  $P_e$  and  $P'_e$  intersect the origins  $O_e, O'_e$ . Pupil planes have a separation distance of  $\Delta_e$ . The object and sensor planes are defined by  $\Pi_o$  and  $\Pi_s$  while  $\mathbf{x}_o$  and  $\mathbf{x}'_o$  represents the point source and main lens real/virtual image positions, with cylindrical coordinates  $(r_o, \theta_o; z_o)$  and  $(r'_o, \theta'_o; z'_o)$  respectively. The object and image distances are  $z_o$  and  $z'_o$ , while  $\alpha_o$  and  $\alpha'_o$  are the zenith polar angles of the chief rays in object and image space.

Let  $\mathbf{x} = \tilde{\mathbf{c}}_o + \mathbf{u}$  and define polar coordinates  $(r'_o, \theta'_o), (\rho, \phi)$  such that  $\tilde{\mathbf{c}}_o - \mathbf{c}_e = (r'_o \cos \theta'_o, r'_o \sin \theta'_o)$  and  $\mathbf{u} = (\rho \cos \phi, \rho \sin \phi) \Rightarrow U(\rho, \phi) = e^{i \frac{k}{a} r'_o \rho \cos(\phi - \theta'_o)} U_o(\rho)$  for radially symmetric  $U_o$ , centred on  $\tilde{\mathbf{c}}_o$ , neglecting the constant phase term  $e^{i \frac{k}{a} (\tilde{\mathbf{c}}_o - \mathbf{c}_e) \cdot \tilde{\mathbf{c}}_o}$

$$\Rightarrow U(\rho, \phi) \propto e^{-ik \tan(\alpha'_o) \rho \cos(\phi - \theta_o)} U_o(\rho)$$

having used that  $\theta'_o = \theta_o + \pi$ ,  $\tan \alpha'_o = \frac{r'_o}{a}$

## 2.2. Theorem (LFC)

Consider Fresnel diffraction from circular apertures of radius  $\tilde{R}_e$  in the plane  $\tilde{\Pi}$ , where  $(v, \omega)$  defines polar coordinates of origin at each aperture centre  $\tilde{\mathbf{c}}_\ell$ . Further let  $(r, \theta)$  represent polar coordinates in the sensor plane  $\Pi_s$  parallel to  $\tilde{\Pi}$  separated at some distance  $b$  and let  $(\rho, \phi)$  represent polar coordinates centred on  $\tilde{\mathbf{c}}_o$ , the chief ray intersection point with  $\tilde{\Pi}$ .

Suppose further that the circular main lens exit pupil has centre  $\mathbf{c}_e$  and is located at a distance  $a$  prior to the microlens entrance pupil plane, with the main lens object and image points given by the polar coordinates  $\mathbf{x}_o = (r_o, \theta_o)$  and  $\mathbf{x}'_o = (r'_o, \theta'_o)$  respectively (see figure 1), while  $U_o(\rho)$  is the radially symmetric aberrated APSF in the *on-axis* case. The angles  $\alpha_o$  and  $\alpha'_o$  are the zenith polar angles of the chief rays in object and image space.

Given that the angular coordinates of  $\tilde{\mathbf{c}}_\ell$  with respect to  $\tilde{\mathbf{c}}_o$  is  $\varphi_\ell = \arctan\left(\frac{(\tilde{\mathbf{c}}_\ell - \tilde{\mathbf{c}}_o) \cdot \hat{\mathbf{e}}_y}{(\tilde{\mathbf{c}}_\ell - \tilde{\mathbf{c}}_o) \cdot \hat{\mathbf{e}}_x}\right)$ , it follows that there exists a shifted coordinate frame  $(\varepsilon, \psi)$  in  $\Pi_s$ , such that the intensity distribution under the  $\ell$ th lens comprises the mirror symmetric property

$$I_\ell(\varepsilon, \varphi_\ell + \psi) = I_\ell(\varepsilon, \varphi_\ell - \psi) \quad (1)$$

and that the optical image point lies on the polar line  $(u, \varphi_\ell)$  in the  $(\varepsilon, \psi)$  frame.

**Proof:** If the wavefront aberration function in the exit pupil is of the form  $W_\ell(v, \omega)$ , then it must follow that there exists a well defined axis of mirror symmetry in the deformation of the wavefront, such that  $W_\ell(v, \varphi_\ell + \omega) = W_\ell(v, \varphi_\ell - \omega)$

Given that  $\rho \cos(\phi - \theta_o) = v \cos(\omega - \theta_o) + \delta_\ell \cos(\varphi_\ell - \theta_o)$  due to the relations between frames  $(\rho, \phi)$  and  $(v, \omega)$ , the incident field  $U(\rho, \phi)$  as given by Lemma 2.1 transforms to the expression

$U_\ell(v, \omega) = e^{-ik \tan(\alpha'_o) v \cos(\omega - \theta_o)} U_{\ell,o}(v, \omega)$ , having neglected the constant phase term  $e^{-ik \delta_\ell \tan(\alpha'_o) \cos(\varphi_\ell - \theta_o)}$ , while

$U_{\ell,o}(v, \omega + \varphi_\ell) = U_{\ell,o}(v, \omega - \varphi_\ell)$  and the transversal euclidean distance  $\delta_\ell = |\tilde{\mathbf{c}}_\ell - \tilde{\mathbf{c}}_o|$ .

Observe  $U_\ell(v, \omega)$  and  $U_{\ell,o}(v, \omega)$  are now  $\ell$ -index dependent as

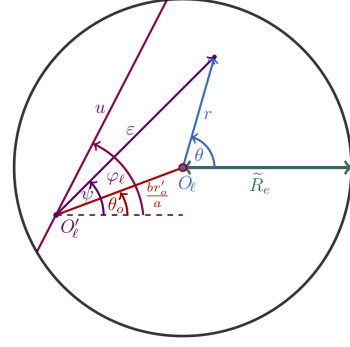


**Figure 2:** Geometry of bipolar coordinate transformation in  $\Pi_s$ : Two true scale polar coordinate frames  $(r, \theta), (\varepsilon, \psi)$  are defined centred on the microimage centre  $O_\ell$  and the displaced origin  $O'_\ell$  due to wavefront tilting. The centres are separated by the distance  $br'_o/a = b \tan(\alpha'_o)$  at an angular orientation of  $\theta_o$ . The microlens radius is  $\tilde{R}_e$ . The distortion line along which the true image point must exist is then represented by the polar line  $(u, \varphi_\ell)$

they are expressed in the local coordinate  $(v, \omega)$  of the microlens. This gives the immediate amplitude distribution behind the lens,  $U'_\ell(v, \omega; 0) = t_\ell(v) P(v) U_\ell(v, \omega)$ , where  $P(v)$  and  $t_\ell(v)$  are the microlens pupil and transmission functions respectively.

From the Fresnel diffraction integral, with the presence of wavefront aberrations, the intensity point spread function is thus

$$I_\ell(r, \theta) = \left| \int_0^{2\pi} \int_0^\infty e^{i \frac{kv^2}{2b}} U'_\ell(v, \omega) e^{ik W_\ell(v, \omega)} \cdot e^{-i \frac{kr}{b} v \cos(\omega - \theta)} v dv d\omega \right|^2 \\ = \left| \int_0^{2\pi} \int_0^\infty e^{i \frac{kv^2}{2b}} t_\ell(v) P(v) U_{\ell,o}(v, \omega) e^{ik W_\ell(v, \omega)} \cdot e^{-ik v (\tan(\alpha'_o) \cos(\omega - \theta_o) + \frac{r}{b} \cos(\omega - \theta))} v dv d\omega \right|^2$$

where the bracketed term in the exponent of the second complex exponential may be expressed as

$$\frac{1}{b} \sqrt{r^2 + (b \tan(\alpha'_o))^2} + 2b \tan(\alpha'_o) r \cos(\theta - \theta_o) \cdot \cos(\omega + \omega'(r, \theta)),$$

for  $\omega'(r, \theta) = \arctan\left(\frac{r}{b} \sin(\theta - \theta_o)\right) - \theta_o$

Introducing a secondary set of polar coordinates  $(\varepsilon, \psi)$  of origin  $O'_\ell$  in  $\Pi_s$  (see figure 2), by the law of cosines and sines

$$\varepsilon = \sqrt{r^2 + (b \tan(\alpha'_o))^2} + 2b \tan(\alpha'_o) r \cos(\theta - \theta_o), \quad \varepsilon \sin(\psi - \theta_o) = r \sin(\theta - \theta_o), \quad \varepsilon \cos(\psi - \theta_o) = r \cos(\theta - \theta_o) + b \tan(\alpha'_o)$$

$$\Rightarrow \omega'(\psi) = \arctan\left(-\frac{\varepsilon}{b} \sin(\psi - \theta_o)\right) - \theta_o = -\psi$$

$$\text{Furthermore, let } G_\ell(v, \omega) := e^{i \frac{kv^2}{2b}} t_\ell(v) P(v) U_{\ell,o}(v, \omega) e^{ik W_\ell(v, \omega)}$$

$$I_\ell(\varepsilon, \varphi_\ell + \psi) = \left| \int_0^{2\pi} \int_0^\infty G_\ell(v, \omega) e^{-i \frac{k\varepsilon}{b} v \cos(\omega - (\varphi_\ell + \psi))} v dv d\omega \right|^2 \quad (2)$$

$$\text{Let } \omega' = \omega - \varphi_\ell \Rightarrow d\omega = d\omega'$$

$$\text{Moreover, clearly } G_\ell(v, \varphi_\ell + \omega) = G_\ell(v, \varphi_\ell - \omega),$$

$$\Rightarrow I_\ell(\varepsilon, \varphi_\ell + \psi) = \left| \int_{-\varphi_\ell}^{2\pi - \varphi_\ell} \int_0^\infty G_\ell(v, \varphi_\ell - \omega') \cdot e^{-i \frac{k\varepsilon}{b} v \cos(\omega' - \psi)} v dv d\omega' \right|^2$$

$$\text{Define } H_\ell(\omega'; \varepsilon, \psi) := \int_0^\infty G_\ell(v, \varphi_\ell - \omega') e^{-i \frac{k\varepsilon}{b} v \cos(\omega' - \psi)} v dv$$

$$\Rightarrow I_\ell(\varepsilon, \varphi_\ell + \psi) = \left| \int_{-\varphi_\ell}^{2\pi - \varphi_\ell} H_\ell(\omega'; \varepsilon, \psi) d\omega' \right|^2 \\ = \left| \int_{-\varphi_\ell}^0 H_\ell(\omega'; \varepsilon, \psi) d\omega' + \int_0^{2\pi - \varphi_\ell} H_\ell(\omega'; \varepsilon, \psi) d\omega' \right|^2$$

For the first integral, let  $\omega = \omega' + 2\pi \Rightarrow d\omega = d\omega'$ .

Then as  $H_\ell(\omega' + 2\pi; \varepsilon, \psi) = H_\ell(\omega'; \varepsilon, \psi)$

$$\implies I_\ell(\varepsilon, \varphi_\ell + \psi) = \left| \int_0^{2\pi} H_\ell(\omega; \varepsilon, \psi) d\omega \right|^2$$

Finally, let  $\omega = \varphi_\ell - \omega' \implies d\omega = -d\omega'$ , we obtain  $I_\ell(\varepsilon, \varphi_\ell + \psi) = \left| -\int_{\varphi_\ell}^{\varphi_\ell - 2\pi} H_\ell(\varphi_\ell - \omega'; \varepsilon, \psi) d\omega' \right|^2$  and thus

$$I_\ell(\varepsilon, \varphi_\ell + \psi) = \left| \int_0^{2\pi} \int_0^\infty G_\ell(v, \omega) e^{-i \frac{kv}{2} v \cos(\omega - (\varphi_\ell - \psi))} v dv d\omega \right|^2$$

$$\implies I_\ell(\varepsilon, \varphi_\ell + \psi) = I_\ell(\varepsilon, \varphi_\ell - \psi)$$

The last step follows from equality of the right-hand side with  $-\psi$  in place of  $\psi$  in eq.(2).

The optical image point  $\mathbf{x}'_\ell$  can be defined as the *centre of mass* of the irradiance distribution  $I_\ell(\varepsilon, \psi)$  in  $\Pi_s$ . To show that this lies on the axis of diffractive mirror symmetry, consider the rotated polar frame  $(\varepsilon, \psi')$  centred on  $\mathbf{O}'_\ell$ , where  $\psi' = \psi - \varphi_\ell$ .

Define  $\tilde{\mathbf{y}}_\ell = (\mathbf{x}'_\ell - \mathbf{O}'_\ell) \cdot (\cos(\varphi_\ell + \pi/2), \sin(\varphi_\ell + \pi/2))^T$ , [i.e. the perpendicular distance of  $\mathbf{x}'_\ell$  from the polar line  $(u, \varphi_\ell)$ ].

Then  $\tilde{y}_\ell \propto \int_{-\pi}^{\pi} \int_0^\infty \varepsilon \sin(\psi') I_\ell(\varepsilon, \psi') \varepsilon d\varepsilon d\psi'$   
 $= \int_0^\infty (\int_0^\pi \sin(\psi') I_\ell(\varepsilon, \psi') d\psi' - \int_{-\pi}^0 \sin(-\psi') I_\ell(\varepsilon, -\psi')) \varepsilon^2 d\varepsilon$   
 having used that  $\sin$  is an odd function and the mirror symmetry property of the irradiance  $I_\ell(\varepsilon, \psi') = I_\ell(\varepsilon, -\psi')$ .

Let  $\psi'' = -\psi' \implies d\psi' = -d\psi''$  but as  $\int_a^b f(t) dt = -\int_b^a f(t) dt$  for the second integral over  $\psi'' \implies \tilde{y}_\ell \propto 0$

**Remarks:** The multiplicative factor  $e^{-ik \tan(\alpha'_o) \rho \cos(\phi - \theta_o)}$  corresponding to wavefront tilting, merely introduces a transversal focal shift to the PSF at the sensor.

### 2.3. Corollary 1

Suppose that the coordinates of each microlens centre with respect to the origin  $O_{\tilde{\Pi}} \in \tilde{\Pi}$  is given by  $\tilde{\mathbf{c}}_\ell = (\tilde{c}_\ell^x, \tilde{c}_\ell^y, 0)^T$ .

Then the cartesian equation for the *distortion line* in  $\Pi_s$  of  $(X_\ell, Y_\ell)$  points, along which the image point exists, takes the form

$$Y_\ell = \tan \varphi_\ell (X_\ell - \tilde{c}_\ell^x - b \tan \alpha'_o \cos \theta'_o) + \tilde{c}_\ell^y + b \tan \alpha'_o \sin \theta'_o \quad (3)$$

**Proof:** Let the coordinates of the origins  $O_\ell$  and  $O'_\ell$  be given by  $\mathbf{O}_\ell$  and  $\mathbf{O}'_\ell$  respectively. As the optical axis of each microlens intersects  $\Pi_s$  at the same transversal coordinates as the microlens centre  $\tilde{\mathbf{c}}_\ell$ , then  $\mathbf{O}_\ell = (\tilde{c}_\ell^x, \tilde{c}_\ell^y)^T$   
 $\implies \mathbf{O}'_\ell \cdot \hat{\mathbf{e}}_x = \tilde{c}_\ell^x + b \tan \alpha'_o \cos \theta'_o$ ,  $\mathbf{O}'_\ell \cdot \hat{\mathbf{e}}_y = \tilde{c}_\ell^y + b \tan \alpha'_o \sin \theta'_o$ ;  
 $\theta'_o := \theta_o + \pi$  (see figure 2).

As proven from the LFC Theorem, as the diffraction pattern possesses an axis of mirror symmetry oriented along the polar line  $(u, \varphi_\ell)$  in  $O'_\ell$ , then the optical image point (centre of mass of the irradiance distribution) must exist on this line.

In cartesian coordinates  $(X_\ell, Y_\ell)$  with respect to the origin of the sensor  $O_s$ , (where  $O_s$  has transversal coordinates that coincides with  $O_{\tilde{\Pi}}$  and  $O_{\Pi_o}$ ), the distortion line can thus be expressed as  $Y_\ell = \tan \varphi_\ell (X_\ell - \mathbf{O}'_\ell \cdot \hat{\mathbf{e}}_x) + \mathbf{O}'_\ell \cdot \hat{\mathbf{e}}_y$

$$\implies Y_\ell = \tan \varphi_\ell (X_\ell - \tilde{c}_\ell^x - b \tan \alpha'_o \cos \theta'_o) + \tilde{c}_\ell^y + b \tan \alpha'_o \sin \theta'_o \quad (4)$$

### 2.4. Corollary 2

The centre of the  $\ell$ -th microimage is given by the coordinates  $\mathbf{c}'_\ell = (1 + \frac{b}{a}) \tilde{\mathbf{c}}_\ell - \frac{b}{a} \mathbf{c}_e$  and all distortions that satisfy eq.(3) are radially towards or away from  $\mathbf{c}'_\ell$ , with  $\varphi_\ell = \arctan\left(\frac{(\tilde{c}_\ell^y - \mathbf{x}'_\ell) \cdot \hat{\mathbf{e}}_y}{(\tilde{c}_\ell^x - \mathbf{x}'_\ell) \cdot \hat{\mathbf{e}}_x}\right)$ .

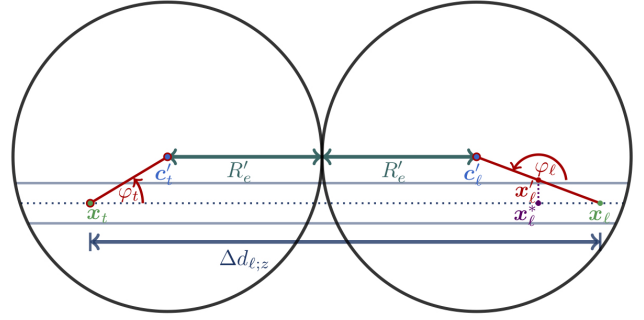


**Figure 3:** Schematic depicting method of disparity estimation by rectifying radial distortions. The radii of the microimages are  $R'_e$  with centres  $\mathbf{c}'_t$  and  $\mathbf{c}'_l$  respectively, while the distortion lines are oriented towards the microimage centres along the angles  $\varphi_t$  and  $\varphi_\ell$ .

**Proof:** The centre of the  $\ell$ -th microimage is given by the image point when  $\tilde{\mathbf{c}}_o = \tilde{\mathbf{c}}_\ell$ . From geometry,  $\tan \alpha'_o = |\tilde{\mathbf{c}}_\ell - \mathbf{c}_e|/a$ , while  $|\tilde{\mathbf{c}}_\ell - \mathbf{c}_e| \cos \theta'_o = (\tilde{\mathbf{c}}_\ell - \mathbf{c}_e) \cdot \hat{\mathbf{e}}_x$  and  $|\tilde{\mathbf{c}}_\ell - \mathbf{c}_e| \sin \theta'_o = (\tilde{\mathbf{c}}_\ell - \mathbf{c}_e) \cdot \hat{\mathbf{e}}_y$   
 $\implies \mathbf{O}'_\ell = (\tilde{c}_\ell^x + b \tan \alpha'_o \cos \theta'_o, \tilde{c}_\ell^y + b \tan \alpha'_o \sin \theta'_o)^T$   
 $\implies \mathbf{O}'_\ell = (1 + \frac{b}{a}) \tilde{\mathbf{c}}_\ell - \frac{b}{a} \mathbf{c}_e$ . Moreover,  $\varphi_\ell$  may take any value on  $[0, 2\pi)$ , and the image point lies on the distortion line through  $\mathbf{O}'_\ell$ , then the image point is uniquely  $\mathbf{O}'_\ell$

$$\implies \mathbf{c}'_\ell = \left(1 + \frac{b}{a}\right) \tilde{\mathbf{c}}_\ell - \frac{b}{a} \mathbf{c}_e \quad (5)$$

To now prove that the distortions are radially centred on  $\mathbf{c}'_\ell$ , we must show that  $\mathbf{c}'_\ell$  satisfies the distortion line equation (3) *independently* of the conjugate point  $\mathbf{x}_o$ . Thus substituting into eq.(3)  $X_\ell = [(1 + \frac{b}{a}) \tilde{c}_\ell^x - \frac{b}{a} c_e^x] \cdot \hat{\mathbf{e}}_x$ , with  $\tan \alpha'_o = |\tilde{\mathbf{c}}_\ell - \mathbf{c}_e|/a$ ,  $|\tilde{\mathbf{c}}_\ell - \mathbf{c}_e| \cos \theta'_o = (\tilde{\mathbf{c}}_\ell - \mathbf{c}_e) \cdot \hat{\mathbf{e}}_x$ ,  $|\tilde{\mathbf{c}}_\ell - \mathbf{c}_e| \sin \theta'_o = (\tilde{\mathbf{c}}_\ell - \mathbf{c}_e) \cdot \hat{\mathbf{e}}_y$ , we obtain,  $Y_\ell = \tilde{c}_\ell^y + \frac{b}{a} [\tan \varphi_\ell (\tilde{c}_\ell^x - \tilde{c}_o^x) + \tilde{c}_o^y - c_e^y]$ .

But  $\tan \varphi_\ell = \frac{\tilde{c}_\ell^y - \tilde{c}_o^y}{\tilde{c}_\ell^x - \tilde{c}_o^x} \implies Y_\ell = [(1 + \frac{b}{a}) \tilde{c}_\ell^y - \frac{b}{a} c_e^y] \cdot \hat{\mathbf{e}}_y$

Conclusively, as the distortion lines all intercept the microimage centre  $\mathbf{c}'_\ell$ , then it is the centre of *radial* distortion!

As the distortion lines intercept both the points  $\mathbf{c}'_\ell$  and  $\mathbf{x}'_\ell$  which are known parameters from measurement, we may re-express

$$\varphi_\ell = \arctan\left(\frac{(\mathbf{c}'_\ell - \mathbf{x}'_\ell) \cdot \hat{\mathbf{e}}_y}{(\mathbf{c}'_\ell - \mathbf{x}'_\ell) \cdot \hat{\mathbf{e}}_x}\right)$$

**Remarks (Lightfield Microscope):** For a telecentric (afocal) main lens such as a microscope objective-tube lens,  $\tilde{\mathbf{c}}_o = M \mathbf{x}_o$ , where  $M = -\frac{f_{tl}}{f_{ob}}$  is the microscope's lateral magnification and  $f_{ob}$ ,  $f_{tl}$  are the focal lengths of the objective and tube lens respectively. But as  $\mathbf{c}_e = \tilde{\mathbf{c}}_o$ , from eq.(5)  $\implies \mathbf{c}'_\ell = \mathbf{c}_\ell$  (i.e. the microlens and microimage centres share the same transversal coordinates).

## 3. RECTIFICATION ALGORITHM

### Outline of the Algorithm

(1) Suppose  $R'_e$  is the radius of microimages while microimage centres  $(\mathbf{c}'_\ell)_{\ell \in \mathbb{N}} \subset \mathbb{R}^2$  lie on a regular lattice that replicates the MLA structure, then given  $\ell \in \mathbb{N}$ ,  $n, m \in \mathbb{Z}$ ,  $\exists \mathbf{e}_1, \mathbf{e}_2 \in \mathbb{R}^2$ , with  $|\mathbf{e}_1|, |\mathbf{e}_2| = 2R'_e$ :  $\mathbf{c}'_\ell = n\mathbf{e}_1 + m\mathbf{e}_2 + \mathbf{t}$  for some  $\mathbf{t} \in \mathbb{R}^2$  (Note: Here  $|\cdot|$  represents the usual Euclidean norm in  $\mathbb{R}^2$ ).

(2) Given a set of point correspondences  $(\mathbf{x}'_\ell)_{\ell \in \mathbb{N}} \subset \mathbb{R}^2$ ,  $\mathbf{x}'_\ell$  is an image point of the  $\ell$ -th microimage if  $|\mathbf{x}'_\ell - \mathbf{c}'_\ell| < R'_e$

(3) Define or construct an *ideal* reference image point for rectification of optical distortions. In particular, define this to be the image point closest to the centre of its microimage (see figure 3). i.e.  $\mathbf{x}_\ell := \mathbf{x}'_\ell$  for some  $t \in \mathbb{N}$ :  $|\mathbf{x}'_\ell - \mathbf{c}'_\ell| = \min_{\ell \in \mathbb{N}} \{|\mathbf{x}'_\ell - \mathbf{c}'_\ell|\}$

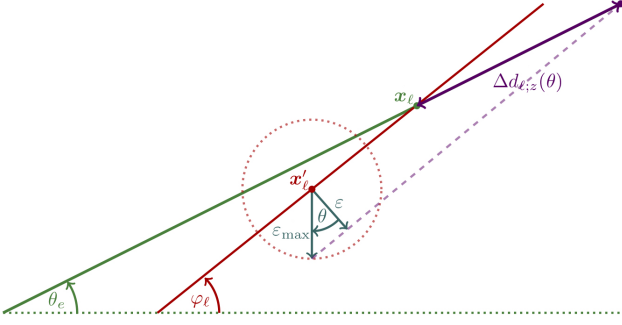


**Figure 4:** Geometrical construction of the weighting function for the handling of outliers due to optical noise. The error in the ideal image point coordinates and thus error in estimated disparity  $\Delta d_{\ell; z}(\theta)$  increases as the gradients of the ideal epipolar line and the distortion line converge.

(It is assumed that the image point  $\mathbf{x}'_t$  of the point correspondences closest to the microimage centre  $\mathbf{c}'_t$  gives the minimal distortion. There is particularly good evidence for this from a theoretical basis under the circumstances that the system is free of optical aberrations).

(4) Find the microimages for which the epipolar lines through  $\mathbf{x}_t$  intersect. i.e. Given  $n \in \mathbb{Z}, \exists p \in \{1, 2\}, \ell \in \mathbb{Z} : \mathbf{c}'_\ell - \mathbf{c}'_t = n\mathbf{e}_p$

(5) Suppose that the identified image point correspondences from a spot detection algorithm are not subject to quantisation. From the LFC Theorem and Corollary 2 regarding the centre of radial distortions, the ideal image points  $\mathbf{x}_\ell$  from the pinhole model can be estimated from the intersection of the ideal epipolar lines with the radial distortion lines (see figure 3).

$$\implies \mathbf{x}_\ell = \mathbf{c}' + \left[ \frac{(\mathbf{x}_t - \mathbf{c}'_t) \cdot \hat{\mathbf{e}}_p}{(\mathbf{x}'_\ell - \mathbf{c}'_\ell) \cdot \hat{\mathbf{e}}_p} \right] (\mathbf{x}'_\ell - \mathbf{c}'_\ell)$$

where  $\hat{\mathbf{e}}_p = \mathbf{e}_p / |\mathbf{e}_p|$

(6) Estimate disparity by considering baselines between the point correspondences in reference to the ideal image point  $\mathbf{x}_t$ . So the disparity between  $\mathbf{x}_t$  and the estimated  $\ell$ -th ideal image point  $\mathbf{x}_\ell$  ( $\ell \in \mathbb{N} \setminus \{t\}$ ) is given by the set of coefficients

$$d_{\ell; z} = 2R_e \left( 1 - \frac{|\mathbf{x}_\ell - \mathbf{x}_t|}{|\mathbf{c}'_\ell - \mathbf{c}'_t|} \right)$$

Using the weighted arithmetic mean, we can estimate the overall disparity by the equation  $d_z = \frac{\sum_\ell w_\ell d_{\ell; z}}{\sum_\ell w_\ell}$  with  $w_\ell \in \mathbb{R}_{\geq 0}, \forall \ell$

(7) From a geometrical construction of how quantisation induces depth errors, we may make the following argument (see figure 4). Let  $\varepsilon_{max}$  be the maximum euclidean distance error in the position of  $\mathbf{x}'_\ell$ , while  $\theta_e$  is the slope of the ideal epipolar line. Furthermore, let  $\beta_\ell = |\varphi_\ell - \theta_e|$  and  $\theta$  be the angle between a line with respect to the perpendicular to the distortion line. From geometry, the error in disparity can be shown to then be  $\Delta d_{\ell; z}(\theta) = \frac{\varepsilon_{max} \cos \theta}{\sin \beta_\ell}$ . If the error in the centroid position due to quantisation can occur with equal probability in any direction about  $\mathbf{x}'_\ell$ , (the measured image point), then the mean absolute deviation in error in disparity around the central point mean can be shown to be  $\bar{\Delta} d_{\ell; z} = \frac{1}{2\pi} \int_0^{2\pi} |\Delta d_{\ell; z}(\theta)| d\theta = \frac{\varepsilon_{max}}{2\pi \sin \beta_\ell} \int_0^{2\pi} |\cos \theta| d\theta = \frac{2\varepsilon_{max}}{\pi \sin \beta_\ell}$ . Thus choose the confidence weighting coefficients for the estimation of disparity to be the reciprocal of this value, so that  $w_\ell = \frac{\pi \sin \beta_\ell}{2\varepsilon_{max}}$

Observe  $\lim_{\beta_\ell \rightarrow 0} w_\ell = 0$  and  $\frac{dw_\ell}{d\beta_\ell} > 0$ , for  $\beta_\ell \in [0, \pi)$

[i.e. the weighting converges to 0 as the gradient of the distortion line converges to that of the ideal epipolar line, and the confidence weighting is strictly increasing with the angular difference

between the two slopes].

## 4. CONCLUSION

We've established a set of generic conditions that give rise to radially distorted microimages in plenoptic cameras and mathematically prove this property in the LFC Theorem. This was shown using Fresnel diffraction theory assuming wavefront symmetries. The centres of radial distortion are shown to be the microimage centre. Under such circumstances, a novel algorithm is proposed for the rectification of sheared curvilinear epipolar lines in these imaging systems. An advantage to this algorithm is that it does not require any advanced modelling of the system's design or imaging properties or any need for a calibration target. This makes our approach appealing from a practical perspective to correct for general complex radial distortions due to aberrations and vignetting. In future work we will extend our preliminary algorithm using a pixel matcher that accounts for the sheared epipolar lines. Simulations using synthetic data will validate the algorithm's performance under the framework of its own assumptions.

## 5. REFERENCES

- [1] Christian Heinze, Stefano Spyropoulos, Stephan Hussmann, and Christian Perwass, "Automated robust metric calibration algorithm for multifocus plenoptic cameras," *IEEE Transactions on Instrumentation and Measurement*, vol. 65, no. 5, pp. 1197–1205, 2016.
- [2] N Zeller, C Noury, F Quint, Céline Teulière, U Stilla, and M Dhome, "Metric calibration of a focused plenoptic camera based on a 3d calibration target," 2016.
- [3] Donald G Dansereau, Oscar Pizarro, and Stefan B Williams, "Calibration and rectification for lenselet-based plenoptic cameras," in *In Proceedings of the 2013 IEEE Conference on Computer Vision and Pattern Recognition (CVPR)*. Citeseer, 2013.
- [4] N Zeller, F Quint, and U Stilla, "Calibration and accuracy analysis of a focused plenoptic camera," *ISPRS Annals of the Photogrammetry, Remote Sensing and Spatial Information Sciences*, vol. 2, no. 3, pp. 205, 2014.
- [5] M Ardebili and A Erdmann, "Point spread and illumination analysis of lightfield cameras," in *2018 25th IEEE International Conference on Image Processing (ICIP)*. IEEE, 2018, pp. 659–663.
- [6] Pat Hanrahan and Ren Ng, "Digital correction of lens aberrations in light field photography," in *International Optical Design Conference*. Optical Society of America, 2006, p. WB2.
- [7] Alessandro Grosso, Kurt Vonmetz, and Toralf Scharf, "Aberrations analysis of a focused plenoptic camera," in *Unconventional Optical Imaging*. International Society for Optics and Photonics, 2018, vol. 10677, p. 106772T.
- [8] Suning Li, Yanlong Zhu, Chuanxin Zhang, Yuan Yuan, and Heping Tan, "Rectification of images distorted by microlens array errors in plenoptic cameras," *Sensors*, vol. 18, no. 7, pp. 2019, 2018.
- [9] Joseph W Goodman, *Introduction to Fourier optics, Third Edition*, Roberts and Company Publishers, 2005.
- [10] Min Gu, *Advanced optical imaging theory, First Edition*, vol. 75, Springer Science & Business Media, 2000.